

# Monolithic Tunable Active Inductor with Independent $Q$ Control

Curtis Leifso, *Student Member, IEEE*, James W. Haslett, *Senior Member, IEEE*, and John G. McRory, *Member, IEEE*

**Abstract**—A 1.1-GHz fully integrated GaAs MESFET active inductor is presented in this paper. Both the inductance and loss resistance are tunable with the inductance independent of series loss tuning. The measured loss resistance is tunable over a  $-10$ - to  $+15$ - $\Omega$  range with a corresponding change in inductance of less than 10% at 100 MHz and less than 4% for frequencies above 500 MHz. The inductance is tunable from 65 to 90 nH. Considerably larger bandwidths can be achieved depending on the fabrication technology employed and the intended application of the circuit.

**Index Terms**—Active inductor, GaAs, MESFET, MMIC, tunable.

## I. INTRODUCTION

A SIGNIFICANT restraint in monolithic-microwave integrated-circuit (MMIC) design stems from the difficulty in realizing an integrated passive inductor with sufficiently high  $Q$  over a broad bandwidth. Large space requirements, low inductance values, and low  $Q$  factors make these inductors unsuitable for precision applications.

Active designs have allowed larger inductance values to be realized. However, the active inductors published to date are limited in that they are often not tunable. When inductance tuning is introduced, the  $Q$  factor usually shows a strong dependence on both the tuning parameter and frequency of operation. As a result, tuning both the inductance and the  $Q$  factor requires an iterative tuning procedure.

One of the most notable  $Q$ -enhancing techniques has been described by Tokumitsu *et al.* in [1]. In this design, a cascode FET arrangement with resistive feedback is used such that when the FET's are matched, the active inductor's loss resistance can be canceled. The resistive feedback described in [1] was replaced with a common-gate FET in [2], which offered improved  $Q$  factor. However, tuning of  $Q$  or the inductance was not easily accomplished.

Alinikula *et al.* [3], [4] described an alternative topology to that given in [2], which offered greater tuning flexibility. With this technique, the effect of finite channel conductance  $g_{ds}$  was examined and a design was proposed that minimized sensitivity to  $g_{ds}$ . Using an FET operating in its linear region as a variable

resistor, the frequency at which maximum  $Q$  occurred could be controlled. For narrow bandwidths, the  $Q$  factor approached 500, however, the loss resistance showed a strong frequency dependence.

A novel resonator design described by Haigh [5] introduced tuning of both the resonant frequency and the  $Q$  factor. A resonant circuit was formed by using two integrators terminated in a capacitance and connected in a feedback loop. Although the resonant frequency remained independent of  $Q$  tuning, the circuit showed a large loss resistance for frequencies below the resonant frequency.

Tuning control of both inductance and  $Q$  factor was also reported in a novel topology proposed by Lucyszyn and Robertson [6]. This design simulated an inductance that was adjustable over a narrow range of values by changing the gate bias voltage of a single FET. The  $Q$  factor could also be tuned to be maximum at an arbitrary frequency. However, as with the previous design, the loss resistance showed an appreciable frequency dependence resulting in very narrow-band performance.

A more recent design presented by Yong-Ho *et al.* [7] expanded on a common  $Q$  enhancement technique using a single FET with lossy inductive feedback. Instead of using a passive feedback inductor, an active inductor circuit was used in this design. The inductance was made tunable over a wide range by varying the loss resistance of the active feedback circuit. Tuning of the  $Q$  factor was accomplished by varying the positive supply voltage for all FET's and could only be set to infinity for a narrow band of frequencies. The loss resistance also varied over a wide range for frequencies outside of this narrow band.

Sussman-Fort *et al.* [8] proposed a unique compensation technique to realize a gyrator with reduced parasitic effects by replacing the terminating impedance with a passive  $RLC$  network. Simulation results confirmed circuit operation as an active inductor over a frequency range from 1 to 3 GHz; however, the passive  $RLC$  network needed to terminate the gyrator is difficult to fully integrate given the high tolerance of passive components on chip. This is further complicated by the need for passive inductors in the terminating impedance, which introduce significant parasitics, thus requiring an iterative procedure to design the gyrator's passive load.

Several techniques using active compensation of lossy passive structures were proposed in separate works by Brucher *et al.* and Sussman-Fort [9], [10] for use in microwave filters. Although these design methods allowed high- $Q$  filters to be realized, many of these techniques were difficult to realize in monolithic form or did not allow the synthesis of a pure inductance for use in other high-frequency applications that require a purely inductive impedance.

Manuscript received March 18, 1999. This work was supported by TRILabs, by The Canadian Microelectronics Corporation, by the Natural Sciences and Engineering Research Council of Canada under Grant OGP000 7776, and by an Industrial Post-Graduate Scholarship.

C. Leifso and J. W. Haslett are with the Department of Electrical and Computer Engineering, The University of Calgary, Alta., Canada T2N 1N4.

J. G. McRory is with TRILabs Calgary, Calgary, Alta., Canada T3K 3V5, and is also with the Department of Electrical and Computer Engineering, The University of Calgary, Alta., Canada T2N 1N4.

Publisher Item Identifier S 0018-9480(00)04667-6.

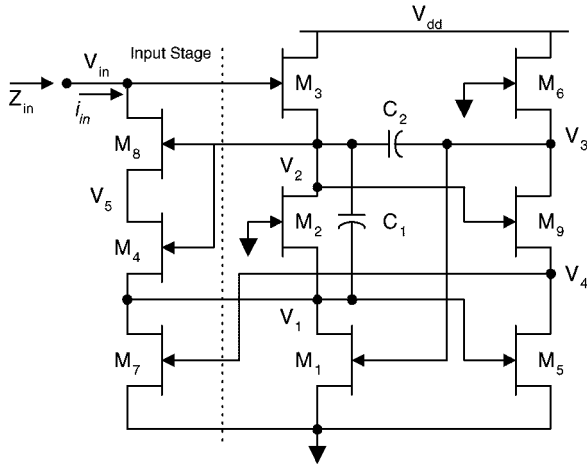


Fig. 1. Active inductor schematic without dc-bias components.

Recently, Sinsky *et al.* [11] presented simulation results for a negative capacitance circuit using conventional second-generation current conveyor design techniques. Tunability of the synthesized impedance could be introduced by replacing resistors in each circuit with an FET biased to give a variable resistance. Each current conveyor was implemented as several cascaded MESFET's such that the equivalent FET had significantly higher gain, thus approaching more ideal behavior of a current conveyor. In order to get sufficiently high gain, however, each current conveyor required large FET's with gatewidths of the order of  $600 \mu\text{m}$ , and two current conveyors were required in addition to off chip biasing components.

A thorough review of many classical two- and three-transistor active inductor circuits in addition to several new topologies has been given by El Khoury [12]. From first-order analysis, these circuits are capable of realizing both positive and negative floating inductance values, but all are limited in their tunability and exhibit many undesirable effects resulting from FET parasitics.

In this paper, an alternative design is presented with more flexible tuning control. With this new technique, the series loss resistance of the simulated inductance is frequency independent over a wide bandwidth. This constant resistance can be varied over a broad range of both positive and negative values with negligible impact on the effective inductance of the circuit. The inductance realized by the circuit is also tunable and remains independent of series loss tuning.

## II. DESIGN AND ANALYSIS

### A. Circuit Design

The schematic of the new active inductor is shown in Fig. 1. Both the simulated inductance  $L_{\text{eq}}$  and the series loss resistance  $R_{\text{loss}}$  are made tunable with two variable capacitors  $C_1$  and  $C_2$ . If  $R_{\text{loss}}$  is to be tunable independently of the inductance, the input impedance expression must be of the form

$$Z_{\text{in}} = j\omega L_{\text{eq}}(C_1) + R_{\text{loss}}(C_1, C_2) \quad (1)$$

which consists of an inductance and a frequency-independent series resistance that are some function of the tuning capacitors

$C_1$  and  $C_2$ . The input impedance will depend primarily on  $C_1$  and  $C_2$  provided they are much larger than the FET parasitic capacitances. This allows the two capacitors  $C_1$  and  $C_2$ , shown in Fig. 1, to be used for tuning of  $L_{\text{eq}}$  and  $R_{\text{loss}}$  where  $R_{\text{loss}}$  can be controlled by  $C_2$  and  $L_{\text{eq}}$  can be independently controlled by varying  $C_1$  while keeping the ratio  $C_1/C_2$  constant.

The circuit can be treated as two independent stages consisting of a voltage-to-current conversion at the input and a six-FET frequency-dependent voltage generator, as shown in Fig. 1. The circuit behaves as a gyrator with a tunable series loss resistance where  $C_1$  is the terminating load whose impedance is to be inverted.

In order to realize an ideal gyrator, the small-signal input current  $i_{\text{in}}$  must be proportional to the product of the port voltage  $v_{\text{in}}$  and the terminating load impedance  $1/(j\omega C_1)$ . Realizing such a circuit is simplified if a small-signal voltage can be generated that is proportional to the load impedance and is a linear function of  $v_{\text{in}}$ . This allows  $i_{\text{in}}$  to be set as required with a simple voltage to current conversion. For the circuit in Fig. 1, the necessary frequency-dependent voltages are given by  $V_1$  and  $V_2$ . The difference  $V_2 - V_1$  is then converted to a proportional current by the input stage to set  $i_{\text{in}}$  as required.

With  $M_1$ ,  $M_2$ , and  $M_3$  in a common-source cascode topology,  $V_1$  and  $V_2$  (shown in Fig. 1) are generated such that if the current into the input port  $i_{\text{in}}$  is set proportional to  $V_1$  or  $V_2$ , both  $L_{\text{eq}}$  and  $R_{\text{loss}}$  will depend on both  $C_1$  and  $C_2$ .

Independence of the inductance from  $R_{\text{loss}}$  can only be achieved provided  $L_{\text{eq}}$  does not depend on both  $C_1$  and  $C_2$ . This is accomplished with a second cascode arrangement consisting of  $M_5$ ,  $M_6$ , and  $M_9$  used to form a feedback loop. This sets the gate voltage of  $M_1$  to  $V_3$ , which is a phase-shifted version of  $V_1$ , causing the transfer functions from the input to  $V_1$  and  $V_2$  to have the same poles.

The input stage formed by  $M_7$ ,  $M_4$ , and  $M_8$  forms a voltage-to-current conversion that sets the input impedance  $Z_{\text{in}}$  inversely proportional to  $V_2 - V_1$ .  $M_4$  sets the small-signal input current equal to  $g_{m4}(V_2 - V_1)$ , resulting in an input impedance with resistive and inductive terms only and with the required form given in (1). FET  $M_9$  has no effect on the feedback voltage  $V_3$  and is only required to set the drain current of  $M_7$  to  $g_{m4}(V_2 - V_1)$ , provided  $M_7$  and  $M_4$  are matched. If  $M_7$  and  $M_4$  are matched, then the voltage-to-current conversion given by  $M_7$ ,  $M_4$ , and  $M_8$  has no impact on node voltages  $V_1$  or  $V_2$  since  $M_4$  injects a current into node  $V_1$  equal to that pulled from the node by  $M_7$ .

FET's  $M_7$  and  $M_8$  are included to reduce the sensitivity of  $Z_{\text{in}}$  to the high channel conductance of the input stage FET's. Alternative stacked FET arrangements can be used to minimize the effects of  $g_{\text{ds}4}$  and  $g_{\text{ds}8}$ . However, the proposed topology reduces the number of FET's required, as well as minimizes the effects of  $M_4$ 's capacitive parasitics.

### B. Circuit Analysis

From Fig. 1,  $Z_{\text{in}}$  can be found from straightforward nodal analysis. Small-signal analysis of the circuit gives  $V_1$  and  $V_2$  as

$$V_1 = \frac{g_{m3}V_{\text{in}}(C_1g_{m5} - g_{m2}C_2 + j\omega C_1C_2)}{Aj\omega + B} \quad (2)$$

$$V_2 = \frac{g_{m3}V_{in}(C_1g_{m5} + g_{m2}C_2 + j\omega C_1C_2)}{Aj\omega + B} \quad (3)$$

where

$$A = C_1C_2(g_{m2} + g_{m3} + 2g_{m5})$$

$$B = C_2(g_{m2}^2 + g_{m2}g_{m3}) + C_1(g_{m5}g_{m3} - g_{m5}g_{m2})$$

assuming that  $C_1$  and  $C_2$  are much larger than the parasitic capacitances of each FET. Both  $V_1$  and  $V_2$  are first-order functions of the input port voltage  $V_{in}$ .

The feedback voltage  $V_3$  causes (2) and (3) to differ only by a sign inverted coefficient in their numerator terms. By subtracting  $V_1$  from  $V_2$ , only a single constant term remains in the numerator expressions, completely removing the inductor's dependence on  $C_2$ . Setting the small-signal input current equal to  $g_{m4}(V_2 - V_1)$ , the equivalent inductance of the circuit  $L_{eq}$  is given by

$$L_{eq} = C_1 \frac{g_{m2} + g_{m3} + 2g_{m5}}{2g_{m2}g_{m3}g_{m4}} \quad (4)$$

which is tunable via  $C_1$  with a series loss resistance given by

$$R_{loss} = \frac{g_{m2}^2 + g_{m2}g_{m3}}{2g_{m2}g_{m3}g_{m4}} + \frac{KC_1}{C_2} g_{m5} \left( \frac{g_{m3} - g_{m2}}{2g_{m2}g_{m3}g_{m4}} \right) \quad (5)$$

which is frequency independent and tunable via  $C_2$ .  $K$  is a dimensionless curve-fitting constant where  $0.3 < K < 0.4$ . This parameter allows the effects of the large FET channel conductances to be modeled without complicating the expression for  $R_{loss}$ . Solving for  $R_{loss}$  using  $V_1$  and  $V_2$ , given in (2) and (3), respectively, results in (5) with  $K = 1$ . Simulation and measurement, however, have shown that the collective effect of parasitics can be accurately modeled with a smaller value of  $K$  since the effect of parasitics is to change the value of  $R_{loss}$  for a given value of  $C_2$ , but the tuning range of  $R_{loss}$  is not altered.

For an appropriate choice of FET dimensions,  $R_{loss}$  can be made tunable over a wide range of both positive and negative resistances. Since (4) is independent of  $C_2$ , the simulated inductance is independent of series resistance tuning.  $R_{loss}$  will also be independent of  $L_{eq}$  tuning provided the ratio  $C_1/C_2$  is held constant as  $C_1$  is varied.

### III. REALIZATION AND PERFORMANCE

The layout of the active inductor is shown in Fig. 2. A  $1\text{-}\mu\text{m}$  GaAs MESFET process was used resulting in a total chip area of  $1.2\text{ mm} \times 1.7\text{ mm}$  for the complete circuit. The test chip was wire bonded to a chip carrier and the input impedance measurements were done with an HP8510C Network Analyzer interfaced through an Elite Test jig.

In order to test the fabricated design, both the inductance and  $Q$  tuning capacitors were built as an array of metal-insulator-metal (MIM) capacitors, which, when connected in parallel, resulted in a capacitance value for  $C_2$  larger than that required for an infinite  $Q$  factor and  $C_1$  set to its largest value. When tuning the input impedance, each capacitor was then reduced in small increments by progressively breaking air bridges supporting the second metal layer between each sub-capacitor, effectively removing it from the parallel con-

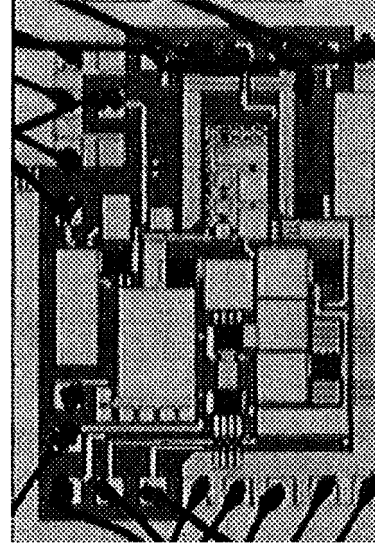


Fig. 2. Die photograph of active inductor. Total area is  $1.2\text{ mm} \times 1.7\text{ mm}$ .

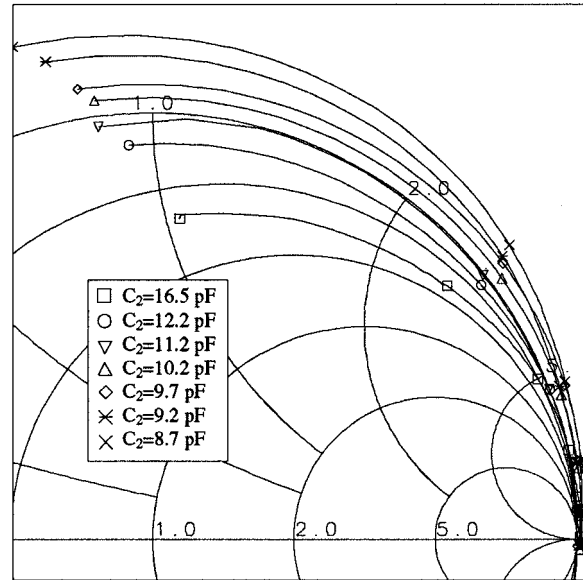


Fig. 3. Measured effect of varying the  $Q$  tuning capacitor  $C_2$  ( $0.1\text{ GHz} < f < 1\text{ GHz}$ ).

nection. As  $C_2$  was decreased,  $R_{loss}$  decreased in accordance with (5), eventually becoming negative. Similarly, as  $C_1$  was decreased,  $L_{eq}$  decreased.

With  $C_1$  fixed to give a constant inductance,  $C_2$  was lowered in small decrements, resulting in the set of impedance plots shown in Fig. 3. The initial value of  $C_2$  caused the first impedance measured to have a large positive loss resistance ( $+15\ \Omega$ ), as predicted by (5). Decreasing  $C_2$  increased the  $Q$  factor, until a sufficiently low loss was realized, as shown in Fig. 3. The simulation results corresponding to the same tuning conditions are shown in Fig. 4.

Continuing to lower  $C_2$  beyond this point made the series loss resistance negative in accordance with (5). The wide loss resistance tuning range is shown in Fig. 5 in comparison to the expected values from both simulation and (5).  $R_{loss}$  can be tuned

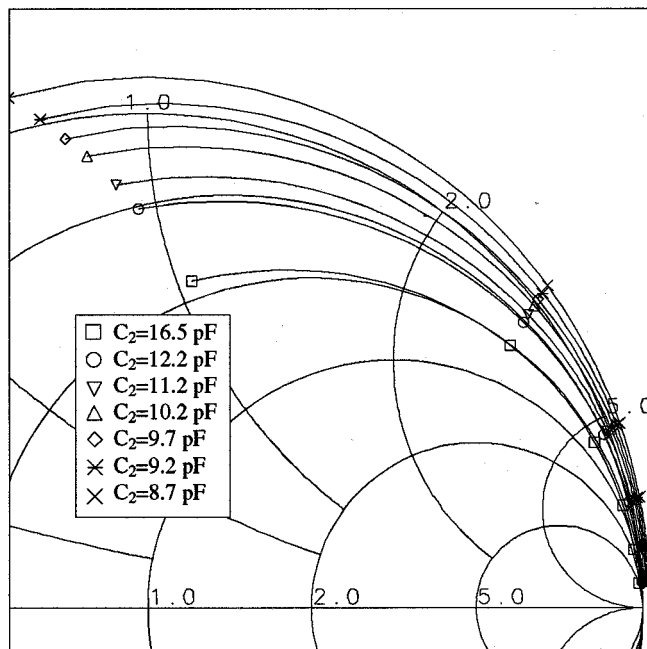


Fig. 4. Simulated effect of varying the  $Q$  tuning capacitor  $C_2$  ( $0.1 \text{ GHz} < f < 1 \text{ GHz}$ ).

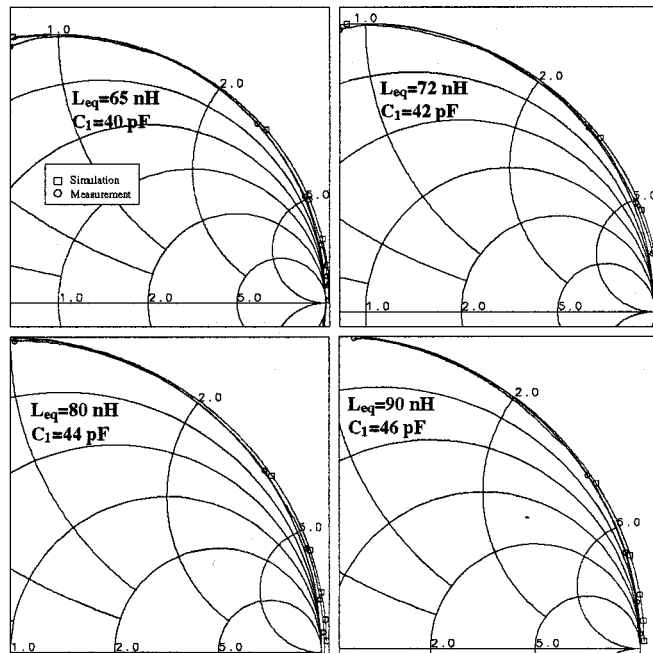


Fig. 6. Simulated and measured effect of varying the inductance tuning capacitor  $C_1$  ( $0.1 \text{ GHz} < f < 1 \text{ GHz}$ ).

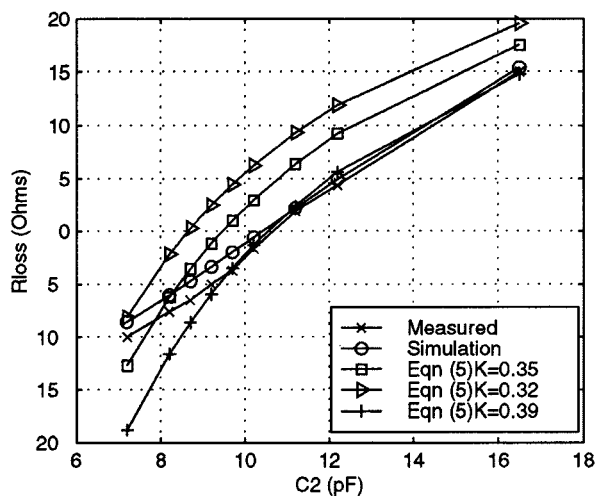


Fig. 5. Effective loss resistance tuning range as a function of  $C_2$ .

over a  $25\text{-}\Omega$  range of both positive and negative resistances corresponding to a  $9.3\text{-pF}$  change in  $C_2$ . The measured and simulated series loss resistances are a near-linear function of the tuning capacitor  $C_2$ . Below  $9 \text{ pF}$ , the assumption that  $C_2$  is much larger than the sum of parasitic capacitances is no longer valid, and  $R_{\text{LOSS}}$  predicted by (5) begins to diverge from measured and simulation results, as shown in Fig. 5. As shown, the effect of  $K$  in (5) is to shift the entire  $R_{\text{LOSS}}$  curve vertically while preserving the effective tuning range as  $C_2$  is varied.

Tuning of the inductance is accomplished by varying  $C_1$ . As  $C_1$  was varied, the ratio  $C_1/C_2$  was held constant to ensure that  $R_{\text{LOSS}}$  stayed constant. Different inductance values were measured and plotted to give the set of curves shown in Fig. 6. The

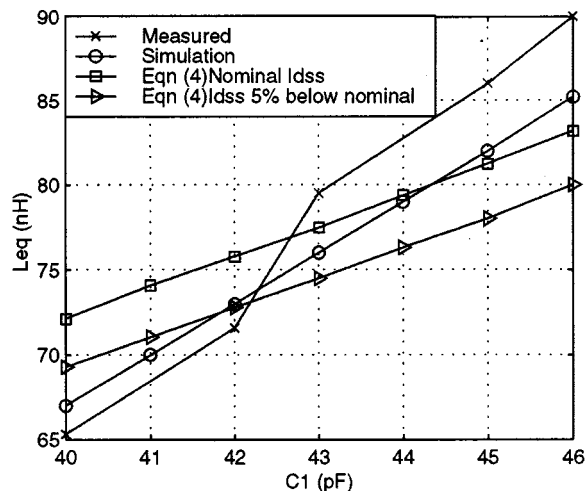


Fig. 7. Inductance tuning range as a function of  $C_1$ .

corresponding simulation results are also shown in Fig. 6 for the same tuning conditions. The excellent agreement between the simulations and measurements was obtained by adjusting the dc gate bias slightly to account for a wide variation in the saturated drain current of the FET's between test chips.

The self-resonant frequency of each inductance value measured was not affected by tuning of  $C_2$ . The measured inductance tuning range is shown in Fig. 7 along with expected values from simulation and (4). As in the case of loss resistance tuning, the inductance dependence on  $C_1$  is also approximately a linear function.

Fig. 7 also shows the expected  $L_{\text{eq}}$  when  $I_{\text{dss}}$  is 5% below the nominal value for the process. As shown, the dynamic tuning

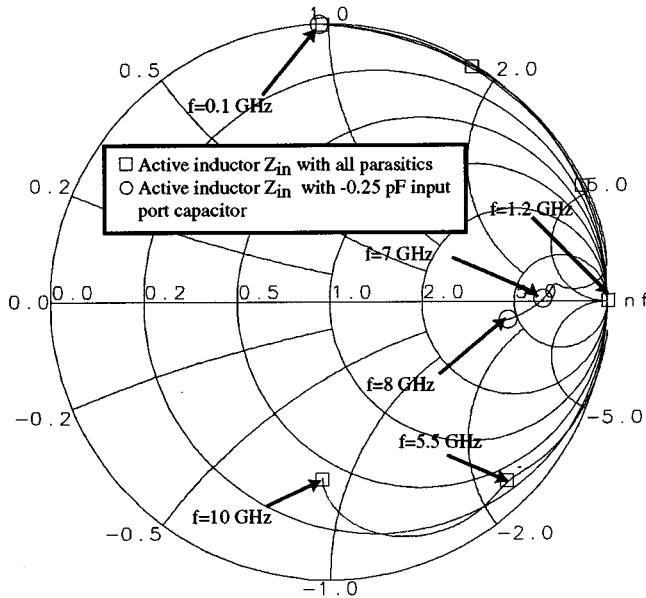


Fig. 8. Simulated effect of bandwidth limiting parasitic capacitors.

range of  $L_{eq}$  is not altered by variations in  $I_{dss}$ . The wider dynamic range measured can be reflected in the simulations by changing the dc-bias conditions in the simulations. The smaller tuning range given by (4) is a result of neglecting the large channel conductance of the FET's. As shown in Figs. 5 and 7, (4) and (5) are reasonably accurate given their simplicity, and proven useful throughout the design of the circuit.

For a fixed inductance of 75 nH and no series loss, the input power level was swept from  $-30$  to  $-0.9$  dBm with negligible change in either the real or reactive component of  $Z_{in}$ . Above  $-0.9$  dBm, both  $L_{eq}$  and  $R_{loss}$  become strong functions of the input power, resulting from a change in the bias points of  $M_4$  and  $M_8$ .

Simulation results show that electronic tuning can be easily introduced without compromising tuning range by replacing both  $C_1$  and  $C_2$  with varactor diodes. Since neither capacitor is grounded, each varactor diode must be placed in series with a fixed capacitance for dc blocking.

#### IV. BANDWIDTH LIMITING PARAMETERS

Analysis, simulation, and measurement results have shown that the active inductor equivalent circuit is an inductor in parallel with a fixed lossy capacitance for frequencies approaching 10 GHz. Simulation results shown in Fig. 8 confirm that it is this small capacitance that limits the self-resonant frequency of the active inductor to 1.1 GHz. Simulations also show that the circuit behaves as an ideal inductor at higher frequencies when this capacitance is removed or significantly reduced. This is also shown in Fig. 8, with an ideal  $-0.25$ -pF capacitor connected from the input to ground. With this shunt negative capacitance, the self-resonant frequency of the active inductor is increased from 1.2 to over 5 GHz.

Analysis and simulation results confirm that it is the capacitive parasitics of FET's  $M_3$  and  $M_8$  that collectively appear as an equivalent capacitance  $C_{eq}$  to ground, as shown in Fig. 9.

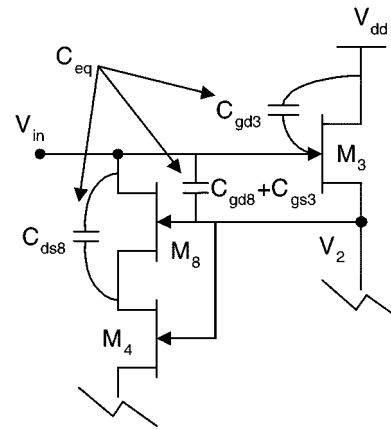


Fig. 9. Bandwidth limiting FET parasitic capacitors.

$C_{ds8}$ ,  $C_{gd3}$ , and  $C_{gd8}$  shown in Fig. 9, are negligible in comparison to  $C_{gs3}$  and, thus,  $C_{gs3}$  dominates the high-frequency performance of the circuit.

The effect of  $C_{eq}$  can be reduced in several ways to considerably extend the effective bandwidth of the inductor. Since a channel length of  $1 \mu\text{m}$  was used for all FET's, the gatewidth required for a reasonable transconductance was also large, resulting in gate-to-source capacitances of the order of 0.6 pF. Simulation results show that a submicrometer process with a gate length less than  $0.5 \mu\text{m}$  increases the inductor's effective bandwidth as a result of significantly lower gate-to-source capacitances.

Alternatively, use of a simple negative impedance converter (NIC) at the input port is being examined. A tunable negative capacitance with sufficiently low conductive loss could provide useful independent tuning of the parallel capacitance or remove it completely if desired. If the inductor is used in applications requiring an LC resonator,  $C_{eq}$  is desirable and can be left alone without any consequence to circuit performance.

#### V. SENSITIVITY TO PARASITICS

Detailed simulations have shown that the sensitivity of  $Z_{in}$  to parasitic contact lead resistance, inductance, and capacitance is negligible. The sensitivity of the realized inductance  $L_{eq}$  to finite drain conductance and parasitic FET capacitances is also very small, resulting in realized inductances that are accurately predicted by (4).

The loss resistance is insensitive to individual FET parasitics, but collectively these parasitics result in a measured  $R_{loss}$  that is not accurately predicted by (5), unless the parameter  $K$  is included. A fixed value of  $K$  between 0.3 and 0.4 results in (5), accurately predicting  $R_{loss}$  over the entire tuning range.

#### VI. CONCLUSION

An active inductor circuit has been developed with tunable inductance and independently tunable series loss resistance. Measurement results confirm the tuning control of both the inductance and loss resistance and the independence of the inductance from loss resistance tuning. Simple analytical expressions have been presented for both the inductance and series loss resistance. Analytic predictions and simulations were found to be

in good agreement with measured results. Electronic tuning of both the inductance and loss resistance can be achieved with varactor diodes.

#### ACKNOWLEDGMENT

The authors would like to thank D. Poulin, Nortel Ottawa, Ottawa, Ont., Canada, G. Rabjohn, Nortel Ottawa, Ottawa, Ont., Canada, and C. Gratton, Nortel Ottawa, Ottawa, Ont., Canada, for many useful discussions and technical support.

#### REFERENCES

- [1] S. Hara, T. Tokumitsu, T. Tanaka, and M. Aikawa, "Broadband monolithic microwave active inductor and its application to miniaturized wide-band amplifiers," *IEEE Trans. Microwave Theory Tech.*, vol. 36, pp. 1920–1924, Dec. 1988.
- [2] S. Hara, T. Tokumitsu, and M. Aikawa, "Lossless, broadband monolithic microwave active inductors," in *IEEE MTT-S Int. Microwave Symp. Dig.*, 1989, pp. 955–958.
- [3] R. Kaunisto, P. Alinikula, and K. Stadius, " $Q$ -enhancing technique for high speed active inductors," in *IEEE Int. Circuits Syst. Symp. Dig.*, 1994, pp. 735–738.
- [4] —, "Monolithic active resonators for wireless applications," in *IEEE MTT-S Int. Microwave Symp. Dig.*, 1994, pp. 1151–1154.
- [5] D. G. Haigh, "GaAs MESFET active resonant circuit for microwave filter applications," *IEEE Trans. Microwave Theory Tech.*, vol. 42, pp. 1419–1422, July 1994.
- [6] S. Lucyszyn and I. D. Robertson, "Monolithic narrow-band filter using ultrahigh- $Q$  tunable active inductors," *IEEE Trans. Microwave Theory Tech.*, vol. 42, pp. 2617–2622, Dec. 1994.
- [7] C. Yong-Ho, H. Song-Cheol, and K. Young-Se, "A novel active inductor and its application to inductance-controlled oscillator," *IEEE Trans. Microwave Theory Tech.*, vol. 45, pp. 1208–1213, Aug. 1997.
- [8] S. Sussman-Fort and L. Billonnet, "MMIC-simulated inductors using compensated gyrators," *Int. J. Microwave Millimeter-Wave Computer-Aided Eng.*, vol. 7, no. 3, pp. 241–249, May 1997.
- [9] A. Brucher, C. Cenac, M. Delmond, F. Delpino, B. Madrangeas, P. Meunier, V. Madrangeas, L. Billonnet, and B. Jarry, "Several methodologies for active filter design at microwaves," *Int. J. Microwave Millimeter-Wave Computer-Aided Eng.*, vol. 7, no. 3, pp. 250–267, May 1997.
- [10] S. Sussman-Fort, "Design concepts for microwave GaAs FET active filters," *IEEE Trans. Microwave Theory Tech.*, vol. 37, pp. 1418–1424, Sept. 1989.
- [11] J. Sinsky and C. Westgate, "New approach to designing active MMIC tuning elements using second-generation current conveyors," *IEEE Microwave Guided Wave Lett.*, vol. 6, pp. 326–328, Sept. 1996.
- [12] S. El Khoury, "The design of active floating positive and negative inductors in MMIC technology," *IEEE Microwave Guided Wave Lett.*, vol. 5, pp. 321–323, Oct. 1995.



**Curtis Leifso** (S'97) was born in Man., Canada, on June 14, 1976. He received the B.Sc. degree in electrical engineering from the University of Calgary, Alta., Canada, in 1997, and is currently working toward the Ph.D. degree in electrical engineering at the University of Calgary.

His research is focused on MMIC design of active resonant circuits for use in microwave filtering applications.



**James W. Haslett** (S'64–M'66–SM'79) was born in Sask., Canada on September 27, 1944. He received the B.Sc. degree in electrical engineering from the University of Saskatchewan, Saskatoon, Sask., Canada, in 1966, and the M.Sc. and Ph.D. degrees from the University of Calgary, Calgary, Alta., Canada, in 1968 and 1970, respectively.

He then joined the Department of Electrical Engineering, University of Calgary, where he is currently a Professor. He was Head of the Department from 1986 to 1997, and has been a consultant to oil-field instrumentation firms for the past 25 years. His current research interests include analog and digital VLSI design, noise in semiconductor devices, high-temperature electronics for instrumentation applications, and RF microelectronics for telecommunications.

Dr. Haslett is a member of the Association of Professional Engineers, Geologists and Geophysicists of Alberta, The Canadian Astronomical Society, The Canadian Society of Exploration Geophysicists, and The American Society for Engineering Education.



**John G. McRory** (S'85–M'87) was born on June 3, 1952. He received the B.Sc. degree in electrical engineering from the University of Alberta, Edmonton, Alta., Canada, in 1986, and the M.Eng. and Ph.D. degrees from the University of Calgary, Calgary, Alta., Canada, in 1993 and 1997, respectively.

In 1986, he joined Novatel Communications in Calgary, Alberta, first as an RF Engineer and Project Manager, and then as the Manager of the Antennas and Systems Group within the Applied Research Group. In 1992, he joined TRILabs, Calgary, Alta., Canada, as a Researcher, and is currently a Chief Scientist, RF Technology. He is also an Adjunct Professor in the Department of Electrical and Computer Engineering, University of Calgary. His current research interests include linear high-power RF amplifiers, nonlinear systems, and device modeling.